DOI: 10.1002/chem.200601817

Controlled Fabrication of Highly Oriented ZnO Microrod/Microtube Arrays on a Zinc Substrate and Their Photoluminescence Properties

Yang Liu, Ying Chu,* Li-Li Li, Li-Hong Dong, and Yu-Jiang Zhuo[a]

Abstract: Well-aligned zinc oxide microrod and microtube arrays with high aspect ratios were fabricated on zinc foil by a simple solution-phase approach in an aqueous solution of ethylenediamine (en). The shape of the ZnO microstructures can be easily modulated from rods to tubes by adding cetyl trimethyl ammonium bromide (CTAB) into the reaction system. Control experiments demonstrate that some reaction parameters, such as the concentration of ethylenediamine, the kind of surfactant, reaction time, and the temperature, all have direct influences on the morphology of the products. Based on the early structure arising from arrested growth (nanosheets), a reasonable mechanism for the growth of ZnO microrods and microtubes has been proposed. The products were characterized by X-ray powder diffraction (XRD), scanning electron microscopy (SEM), transmission electron microscopy (TEM), and photoluminescence emission.

Keywords: crystal growth · nanostructures · semiconductors · surfactants · zinc

Introduction

Recently, one-dimensional (1D) semiconductor nano-/microstructures have been extensively studied owing to their fundamental properties, which make them potentially ideal functional components for nanometer-scale electronic and optoelectronic devices.[1–4] It is well documented that the optoelectronic and chemical properties of inorganic nano/micro-crystals depend strongly on their morphologies, thus, the design and controlled synthesis of 1D nano-/microstructures with different morphological configurations on a large scale is very important from the viewpoint of both science and technology.[5–6] Zinc oxide is one of the most important functional semiconductor materials, because it has a direct and wide band gap of 3.37 eV at room temperature, together with a large excitation binding energy (60 meV), it exhibits near-UV emission, and has transparent conductivity at room temperature and above. The noncentral symmetrical crystallographic structure of ZnO can lead to piezoelectricity as well as pyroelectricity, which make it a promising candidate for building electromechanically coupled sensors and transducers.[7] Shrinking ZnO to 1D nano-/microstructures is expected to create possibilities in a wide range of applications, for example, room-temperature ultraviolet (UV) lasers,[8] blue-ultraviolet region optoelectronic devices,[9] sensors,[10] photocatalysts,[11] piezoelectric transducers and actuators,[12] solar cells,[13] and field-emission devices.[14]

Since the first report of ultraviolet lasing from ZnO nanorods,[8] substantial effort has been devoted to the development of novel synthetic methodologies for 1D ZnO nanostructures, and many methods, including vapor–liquid–solid,[15] vapor–solid,[16] chemical vapor deposition,[17] template-assisted,[18] and other solution processes[19–21] have been used to produce all kinds of 1D ZnO entities. Moreover, the large-scale controllable growth of well-aligned ZnO nanowire, nanorod, or nanoneedle arrays has also been realized on a variety of substrates,[22–24] which is very important for device applications. Although gas-phase deposition is one of the principal technologies for the growth of high quality and aligned 1D ZnO nano-/microstructures, the process is expensive and consumes high levels of energy. Recently, chemical solution-phase methods have been found to be more attractive because they can be carried out at moderate temperatures, require simple manipulations, and they have good potential for scale-up. Han et al. successfully fabricated highly oriented hexagonal ZnO nanotube arrays on ZnO-film-coated (arbitrary) substrates on a large scale.[22a] This is regarded as an important work because the tubular form is

[a] Dr. Y. Liu, Prof. Y. Chu, L.-L. Li, L.-H. Dong, Y.-J. Zhuo
Department of Chemistry, Northeast Normal University
Changchun, Jilin 130024 (P.R. China)
Tel: (+86) 431-8509-9320
E-mail: chuying@nenu.edu.cn

Supporting information for this article is available on the WWW under http://www.chemeurj.org/ or from the author.

generally limited to layered materials such as carbon nanotubes and would indicate that, although uncommon, it is possible to obtain the tubular structure on a large scale for nonlayered ZnO materials. Here, we present a simple route for the growth of well-oriented 1D ZnO microstructure arrays over a large area by direct oxidation of zinc foil in an aqueous solution of ethylenediamine. Furthermore, the shape of the ZnO microstructures can be easily modulated from rods to tubes by adding surfactant into the reaction system. This is a convenient and low-cost method for the control of the shape and synthesis of 1D ZnO microstructures.

Results and Discussion

The morphology of an array of ZnO microrods grown by our method was characterized by scanning electron microscopy (SEM). Overall, the product layer produced on the Zn substrate is highly uniform over a large area (Figure 1a). A tilted view of the array of rods shown in Figure 1b suggests that these ZnO microrods are oriented approximately perpendicular to the surface of the substrate and are typically 30 μm in length. Figure 1c is a magnified image, clearly showing the microrods grown in a dense array with a mean diameter of 0.5–1.0 μm, and, in addition, an exceptionally large aspect ratio is thus achieved (in the range of 30–60). The inset of Figure 1c shows that the ZnO microrods possess well-defined hexagonal-prism morphology. The X-ray diffraction (XRD) pattern of the product layer on the Zn substrate (Figure 1d) suggests that the crystallographic phase of the array of ZnO microrods belongs to the Wurtzite-type (space group: $P63/mc$, JCPDS: 36-1451), and the measured lattice constants c_o and a_o of this hexagonal phase are 5.21 and 3.25 Å, respectively ($c_o/a_o = 1.60$). Notably, the (002) diffraction peak at $2\theta = 34.4°$ is enhanced and much stronger than the other peaks, suggesting a preferential orientation of the crystals along the c axis of the ZnO microstructures, perpendicular to the substrate surface. The composition of the array of ZnO microrods was analyzed by an energy dispersive X-ray spectroscopy (EDS) study (Supporting Information, SI-1). This study revealed the presence of Zn and O as the only elementary components and indicated a slight oxygen deficiency (Zn/O ≈ 1:1, atomic ratio). No traces of other elements were detected; this indicates that the ethylenediamine was completely removed during the growth and washing process.

Although the majority of the ZnO microrods were grown on the zinc foil, individual microrods can be separated by using sonication. Figure 2 shows a typical transmission electron microscopy (TEM) image of a free-standing ZnO microrod, which is in good agreement with the SEM results,

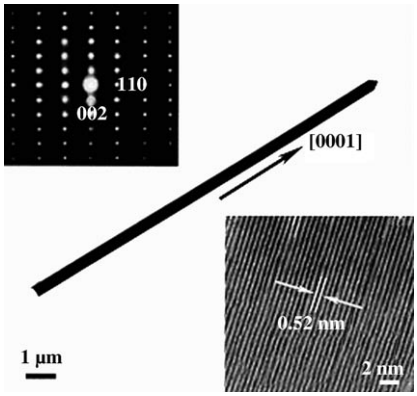

Figure 2. TEM, SEAD, and HRTEM images of a ZnO microrod.

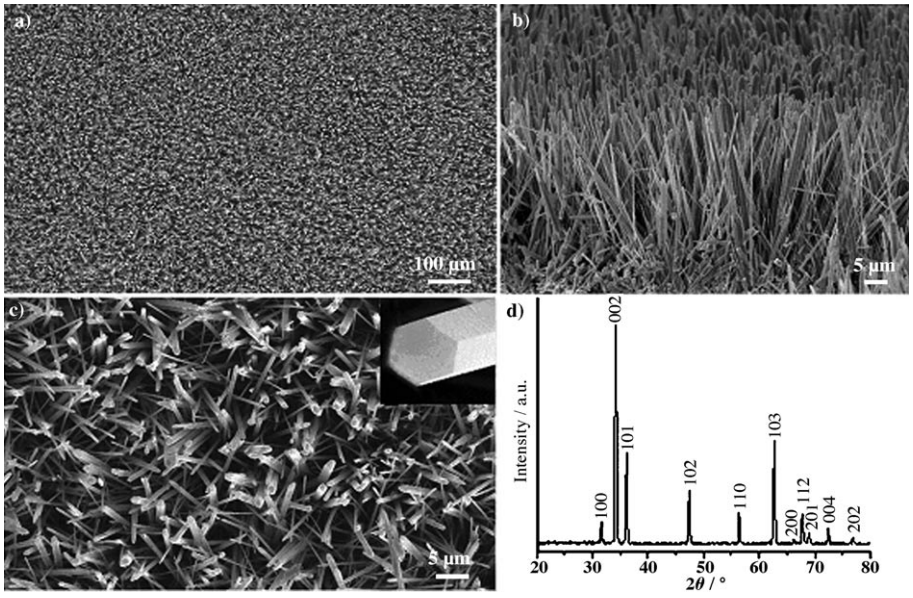

Figure 1. The a) overview, b) tilted view, c) magnified view SEM images, and the d) XRD pattern of an array of ZnO microrods on a zinc substrate.

exhibiting the rodlike morphology with a pointed tip. The individual microrod has a uniform diameter along its entire length; this indicates that the growth anisotropy along the $+c$ axis is strictly maintained throughout the process. In particular, no branching is observed, which implies that the ZnO microrods were grown from spontaneous nucleation and contain high crystal perfection.[22a] Furthermore, the selected area electron diffraction (SAED) pattern and the high-resolution TEM (HRTEM) image recorded at the tip of the representative ZnO microrod indicates its single crystal nature. The features of the diffraction pattern show that the

preferred growth of the ZnO microrods is in the [0001] direction. The displayed lattice spacing of 0.52 nm perpendicular to the microrods axis corresponds to the interplanar spacing of the (002) planes of ZnO, which also indicates that the [0001] direction is preferred for growth.

The amount of ethylenediamine (en) is a critical parameter for the growth of the ZnO microrods. By using only a small amount of ethylenediamine (3.5 mL), an array of dense, long rods assembled from nanosheets forms (Figure 3a–c), rather than an array of smooth rods. Additionally, a proportion of the sample did not grow perpendicular to the substrate. The XRD pattern shown in Figure 3d reveals that the sample obtained in this case was $Zn(OH)_2$ (marked with ■, JCPDS 74–0094) as result of the side reaction $[Zn(OH)_4]^{2-} \rightarrow Zn(OH)_2\downarrow + 2\,OH^-$, and the peaks marked with stars are attributed to the zinc foil (JCPDS 04-0831). The stoichiometry of the sample was investigated by using EDS, which reveals the atomic ratio of $Zn/O \approx 1:2$ (Supporting Information SI-2).

Interestingly, if cetyl trimethyl ammonium bromide (CTAB) is added to the reaction mixture and the other reaction conditions are kept similar, an array of tubelike ZnO structures can be grown on the Zn substrate (Figure 4 illustrates the morphology and structural characterization results). An array of dense, highly oriented ZnO microtubes was obtained when the synthesis was carried out in a solution containing 0.02 M CTAB (Figure 4a,b). The length of the ZnO microtubes was found to be in the range of 20–25 μm. The magnified images of the microtubes are shown in Figures 4c and 5, from which we find that the walls of the tubes are not smooth, but are constructed by numerous nanosheets. The wall thickness and the diameter of the inner cavity are 200 and 300–500 nm, respectively. Recently, Liu et al. synthesized ZnO microtubes that have a similar morphology,[25] but the orientation of the array was not described. Figure 4d is the XRD pattern of the ZnO microtube array.

We found that the morphology of the ZnO microstructures is sensitive to different surfactants. Typical SEM images of the ZnO sample obtained from the reaction system containing 0.02 M sodium dodecyl sulphate (SDS) are shown in Figure 6. A low-magnification SEM image of the densely packed candy-rodlike structures is illustrated in Figure 6a. The magnified images of the ZnO candy-rods clearly demonstrate that these rods are constructed by many nanosheets (Figure 6b, and SI-3 in the Supporting Information),

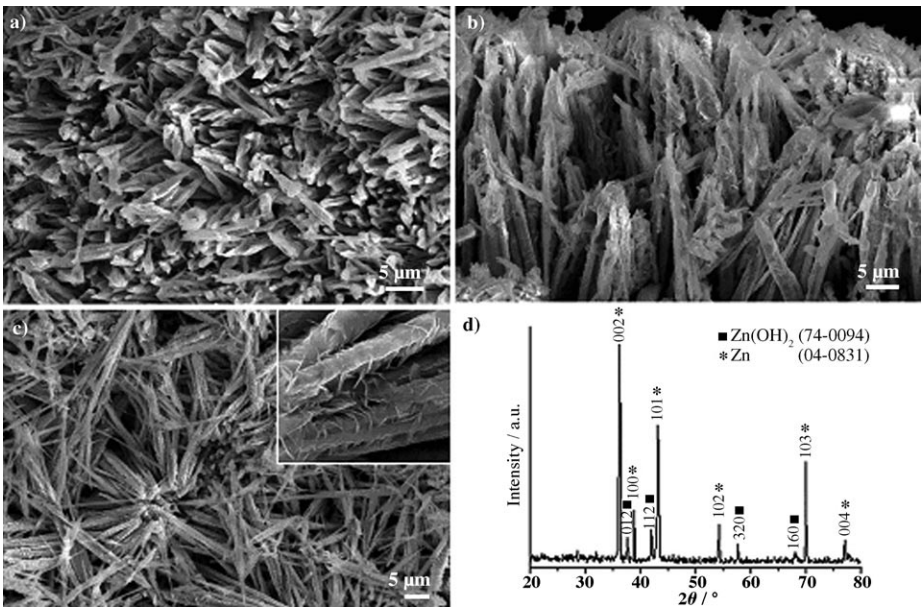

Figure 3. The a) overview and b) tilted view SEM images of an aligned array of $Zn(OH)_2$ microrods. c) SEM image of $Zn(OH)_2$ microrods that have fallen on zinc foil. d) XRD pattern of the $Zn(OH)_2$ microrods.

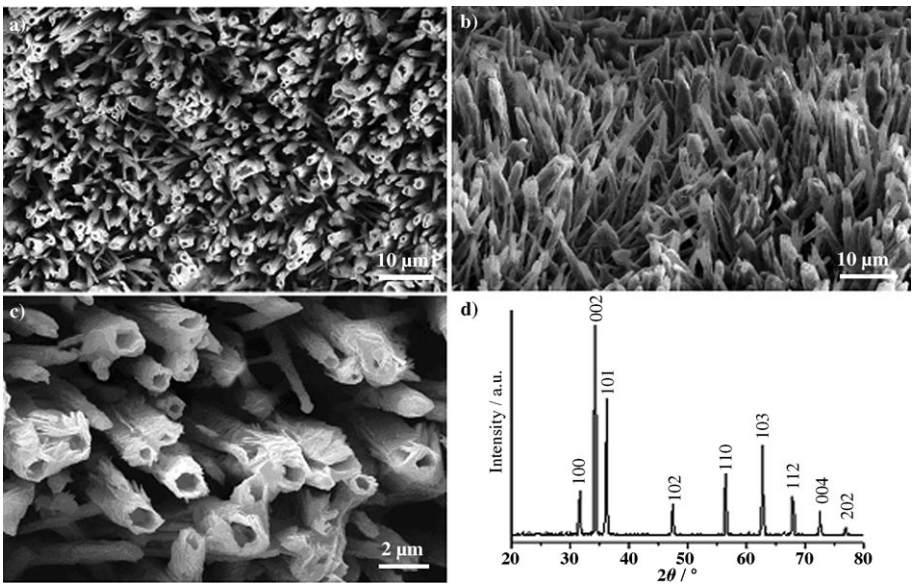

Figure 4. The a) overview, b) tilted view, c) magnified view SEM images and the d) XRD pattern of the array of ZnO microtubes on zinc foil, obtained with the addition of 0.02 M CTAB into the reaction system.

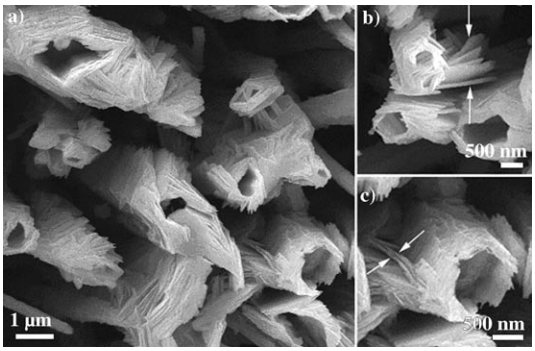

Figure 5. High-magnification SEM images of ZnO microtubes.

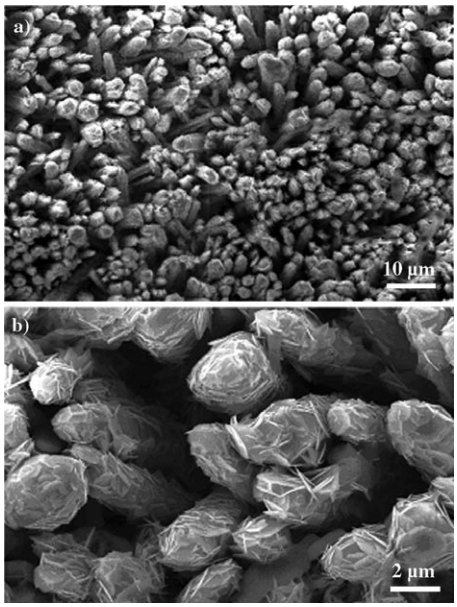

Figure 6. a) Overview and b) magnified view of an array of ZnO candy-rods on zinc foil obtained with the addition of 0.02 M SDS into the reaction system.

which is similar to the phenomenon observed during the preparation of the ZnO microtubes.

Based on the above results, we have found that the nanosheets have a direct relationship with the final morphology of the samples. To trace the morphological evolution of the ZnO samples, an experiment at low temperature (120 °C) was carried out while keeping the other reaction conditions the same as those used up to this point (the reaction conditions can also be found in the Experimental Section). Only a mass of nanosheets with the thickness of 80–100 nm were prepared from this reaction (Figure 7a), which confirms that the nanosheets are the preformed nanostructure. To determine the crystal structure of an individual nanosheet, systematic TEM imaging and diffraction analyses were conducted. A TEM image of several nanosheets, which shows their hexagonal shape, is seen in Figure 7b. The hexagonal electron diffraction spots shown in the SAED pattern are a single crystal [0001] pattern of ZnO (Figure 7c), which reveals that the top and bottom surfaces of the nanosheet are a pair of (0001) and (000-1) *c* planes, though the six side facets are {10–10}. Similar ZnO nanosheet structures have also been observed in the early stages of the preparation of well-aligned ZnO nanorod arrays on zinc foil in ethanol.[24b] SEM images of the sample prepared in a contrast experiment at a reaction temperature of 135 °C (higher than that for nanosheets, but lower than that for microrods) were recorded, and we found that an array of semi-microrods formed from the layer-by-layer stacking of nanosheets (Figure 8).

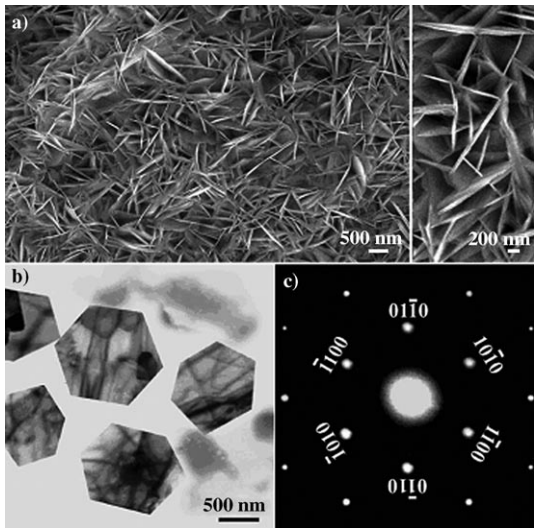

Figure 7. The a) SEM image, b) TEM image, and c) SAED pattern of ZnO nanosheets obtained at 120 °C.

The SEM observation implies that the ZnO microrods, microtubes, and candy-rods all evolved from the nanosheets. Based on the crystal habit of wurtzite ZnO, the growth rates

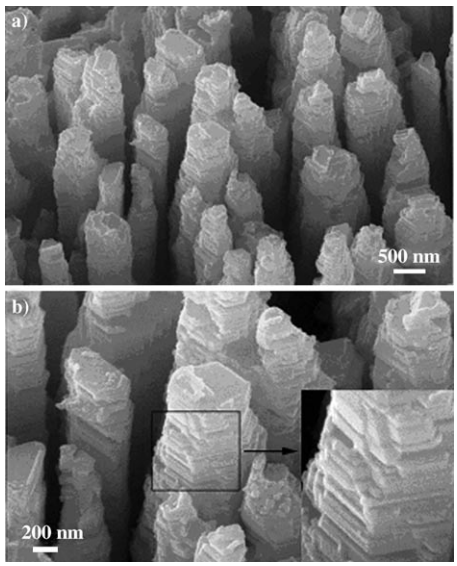

Figure 8. SEM images of an array of semi-microrods obtained at $T=$ 135 °C.

of the different family of planes follow the sequence (0001) > (10-11) > (10-10), and conventionally, the more rapid the growth rate, the quicker the disappearance of the plane. However, under certain circumstances the growth along the [0001] direction disappears altogether, and the planes that have higher Miller indices and lower specific surface energy become preferred.[24c] For the nanosheets we obtained, the (0001) plane, the most rapid-growth-rate plane, dominates large areas of the nanosheets, which are considered to be metastable structures. In this contrast experiment, the lower reaction temperature we employed (120 °C) caused the reaction to proceed much more slowly, and hence, the initial nuclei had sufficient time to grow in the lateral directions, resulting in the formation of nanosheets (Figure 7). Once the reaction temperature has risen to 135 °C, these metastable nanosheets will stack together to lower the system energy and form an array of semi-microrods along with the sheets (Figure 8). Further elevation of the reaction temperature to 160 °C causes these nanosheets to penetrate each other through the coalescence mode and Ostwald ripening, thus microrods with smooth surfaces are formed (Figure 1). Similar layer-by-layer stacking processes from ZnO nanosheets to nanorods have also been observed by other groups.[19d,24b]

The putative reactions relevant to the growth of ZnO structures in an ethylenediamine (en) solution with Zn foil as a reactant can be simply represented by the following reactions (Equations (1)–(4)):

$$Zn + O_2 + 2\,H_2O \rightarrow Zn^{2+} + 4\,OH^- \quad (1)$$

$$Zn^{2+} + 2\,en \rightarrow [Zn(en)_2]^{2+} \quad (2)$$

$$[Zn(en)_2]^{2+} + 4\,OH^- \rightarrow [ZnO_2]^{2-} + 2\,en + 2\,H_2O \quad (3)$$

$$[ZnO_2]^{2-} + H_2O \rightarrow ZnO + 2\,OH^- \quad (4)$$

To grow ZnO structures from zinc foil in solution, basic conditions are necessary. Bidentate ethylenediamine can offer a basic medium, and also perform two other major roles in the growth of ZnO microrods. First, in the case of adding the neutral en molecule, the electrostatic force between the positive polar plane of (0001) and the negative $[ZnO_2]^{2-}$ growth unit is much stronger than the adsorption affinity between the (0001) plane and the neutral en molecule. Therefore, adsorption of the en molecule and $[ZnO_2]^{2-}$ should occur on the lateral {10-10} surfaces group and the (0001) face, respectively. Thus, the radial enlargement of the rods may be largely inhibited owing to the strong chelating ability of en towards the divalent zinc species, and the crystal growth rate along the *c* axis is enhanced.[21d] Second, en could also work as a transport carrier in Ostwald ripening. The sample prepared by using a shorter reaction time of 8 h clearly has a terraced structure (all other reaction conditions were kept the same as those in Experimental Section in the Supporting Information, SI-4), which implies the presence of atomic steps on the side crystallographic planes. During the prolonged reaction the effects of Ostwald ripening become pronounced, as evidenced in the transformation of the terraced morphology to the parallel prismlike planes. The complexing agent (en) in solution could act as a carrier via formation of $[Zn(en)_2]^{2+}$ for zinc transport from one location to another in ripening ZnO rods (i.e., dissolution and then redeposition). Apparently, zinc cations located in the steps and terraces could be more easily dissolved in this complexation process. The zinc complex species in the solution phase are more attracted to adsorption sites with high surface energy (i.e., the (0001) plane) in the subsequent redeposition, which results in the smoother ZnO microrods with uniform diameters.[20d]

CTAB plays an important role in the growth process of ZnO microtubes. When the concentration of CTAB reaches 0.02 M, rodlike capsules of CTAB are generated in the saturation solution. ZnO nanosheets will be adsorbed and stacked up around the circumference of the CTAB capsules as a result of the coulomb-force action between $[ZnO_2]^{2-}$ and cationic surfactant CTAB, and to lower the energy of the reaction system. Certainly, the coalescence mode and Ostwald ripening also exist among the nanosheets during the formation of the ZnO microtubes, therefore, some nanosheets penetrate each other and grow together, as shown in Figure 5. On the other hand, the additional adsorption of CTAB onto the ZnO surfaces (primarily on negative sites, complementary to en-adsorbed positive Lewis acid sites)[20d] results in a certain degree of sheetlike morphology followed by the formation of an array of ZnO microtubes (Figures 4 and 5). Recently, the structure-directing effects of surfactants on CuO nanocrystals prepared on copper foils has also been discussed.[26]

The study of the luminescent properties of these ZnO structures can shed some light on defects in the ZnO crystals and their potential as photonic materials. The room-temperature photoluminescence (PL) spectrum recorded from the array of ZnO microrods is shown in Figure 9a. A sharp and strong UV peak at 3.26 eV ($\lambda = 380$ nm) dominates the PL spectrum, and a weak and broad-green band is found in the range of 2.07–2.95 eV ($\lambda = 420$–600 nm). The UV band emission of the array of ZnO microrods can be assigned to the emission from a free exciton under low excitation intensity,[27] and the weak peaks in the green band possibly originate from the electron transition from the level of the ionized oxygen vacancies to the valence band.[28] The intensity of the deep-level emission is determined by the concentration of the oxygen vacancies in the ZnO crystal.[29] Therefore, the strong and intense UV emission, the weak emission related to the vacant ionized-oxygen levels, and the absence of the well-known stronger and broader emission in the yellow-green band[28] in the PL spectrum illustrate the good crystallization quality and high stoichiometric nature of the obtained array of ZnO microrods. We carried out additional room-temperature PL measurements of the array of ZnO microtubes. The emission spectrum shown in Figure 9b displays a sharp UV emission, and the intensity of the defect-related green emission increases. It is generally

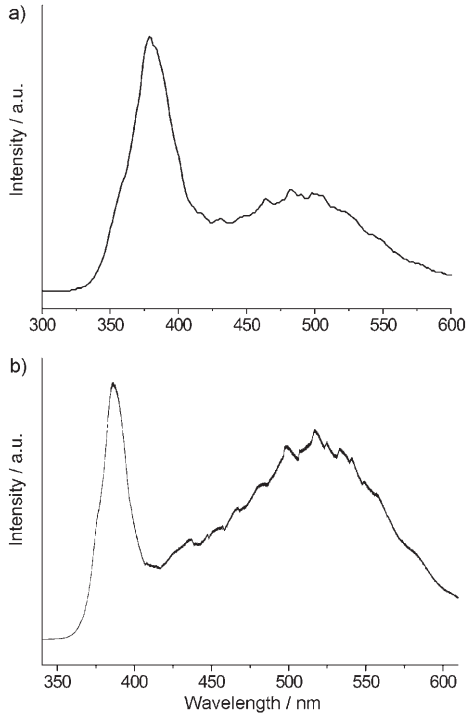

Figure 9. Room-temperature PL spectra of the a) array of ZnO microrods and the b) array of ZnO microtubes.

accepted that the green emission results from the recombination of a photogenerated hole that has a singly ionized charge state within a specific defect.[28] Although the PL spectrum is clear, it is reasonable to predicate that a few crystal defects exist in the array of ZnO microtubes. The PL spectrum of the array of ZnO candy-rods shown in Figure 6 (and in the Supporting Information, SI-5) and the emission spectrum gives a wide band emission covering the blue and green regions, indicating that lots of oxygen vacancies or interstitial Zn centers are present in the sample. The emission spectra of the products synthesized under different conditions are dramatically different from each other, verifying that the optical properties of ZnO crystals are very sensitive to the morphology and preparation conditions.

Conclusion

In summary, highly oriented ZnO microrod/microtube arrays have been successfully fabricated by simple oxidation of a solution of zinc foils in ethylenediamine under hydrothermal conditions (without surfactant for an array of microrods and with surfactant, CTAB, for an array of microtubes). Through changing some reaction parameters, such as the concentration of ethylenediamine, the kind of surfactant, reaction time, and the temperature, ZnO microstructures that have different morphologies were obtained. The SEM observations has allowed for the growth and mechanism for controlling the shape of the structures to be discussed in detail. The PL emission spectra for ZnO microrods and microtubes are different, which confirms that the optical properties of ZnO crystals are very sensitive to the morphology and preparation conditions. It is reasonable to expect that this simple method can easily be scaled up to fabricate various ZnO nano-/microstructures for important applications over a large range of nanotechnologies.

Experimental Section

Materials: The reagents used in this work, including ethylenediamine and ethanol, were of analytical reagent grade and were purchased from the Beijing Chemical Factory, China. Zinc foils ($10\times10\times0.5$ mm, 99.9%) were pretreated by sonication in ethanol for 5 min and dried by using a dry nitrogen stream.

Synthesis: In a typical procedure, a piece of clean zinc foil was immersed in a solution of en (11 mL) and water (24 mL) in a Teflon-lined stainless steel autoclave (50 mL) followed by heating at a constant temperature of 160 °C for 24 h. After the hydrothermal treatment, the resulting zinc foil was taken out and thoroughly rinsed with ethanol and dried in air for further characterization. It is worth noting that this process had high reproducibility and high yield.

Characterization: The XRD pattern was recorded by using a Rigaku D/max 2500 V PC diffractometer ($Cu_{K\alpha}$ radiation). The SEM data were collected by using a XL30 ESEM-FEG microscope at an accelerating voltage of 15 kV. The TEM observations were performed by using a JEOL 2010 instrument. The final zinc foil was sonicated in ethanol for 10 min and the suspension was dropped on the carbon-coated Cu grid, followed by evaporation of the solvent in the ambient environment. The PL emission spectra were measured by using an excitation wavelength of 325 nm with a power of 50 mW, and performed on a LABRAM-UV Raman microspectrometer (Jobin Yvon).

Acknowledgements

This work was financially supported by the National Natural Science Foundation of China (no. 20573017), the Science Foundation for Young Teachers of Northeast Normal University (no. 20060306) and Analysis and Testing Foundation of Northeast Normal University.

[1] M. S. Gudiksen, L. J. Lauhon, J. F. Wang, D. C. Smith, C. M. Lieber, *Nature* **2002**, *415*, 617.
[2] W. I. Park, Y. H. Jun, S. W. Jung, G. C. Yi, *Appl. Phys. Lett.* **2003**, *82*, 964.
[3] X. Duan, Y. Huang, R. Agarwal, C. M. Lieber, *Nature* **2003**, *421*, 241.
[4] Y. Cui, Q. Q. Wei, H. K. Park, C. M. Lieber, *Science* **2001**, *293*, 1289.
[5] a) Z. W. Pan, Z. R. Dai, L. Xu, S. T. Lee, Z. L. Wang, *J. Phys. Chem. B* **2001**, *105*, 2507; b) F. Kim, S. Connor, H. Song, T. Kuykendall, P. D. Yang, *Angew. Chem.* **2004**, *116*, 3759; *Angew. Chem. Int. Ed.* **2004**, *43*, 3673.
[6] a) X. S. Fang, C. H. Ye, L. D. Zhang, Y. H. Wang, Y. C. Wu, *Adv. Funct. Mater.* **2005**, *15*, 63; b) X. Q. Meng, D. X. Zhao, J. Y. Zhang, D. Z. Shen, Y. M. Lu, Y. C. Liu, X. W. Fan, *Chem. Phys. Lett.* **2005**, *407*, 91.
[7] P. X. Gao, C. S. Lao, Y. Ding, Z. L. Wang, *Adv. Funct. Mater.* **2006**, *16*, 53.
[8] M. H. Huang, S. Mao, H. Feick, H. Yan, Y. Wu, H. Kind, E. Weber, R. Russo, P. Yang, *Science* **2001**, *292*, 1897.
[9] J. Johnson, H. Yan, P. Yang, R. Saykally, *J. Phys. Chem. B* **2003**, *107*, 8816.
[10] T. Shibata, K. Unno, E. Makino, Y. Ito, S. Shimada, *Sens. Actuators A* **2002**, *102*, 106.

[11] H. Yumoto, T. Inoue, S. J. Li, T. Sako, K. Nishiyama, *Thin Solid Films* **1999**, *345*, 38.
[12] X. Y. Kong, Z. L. Wang, *Nano Lett.* **2003**, *3*, 1625.
[13] K. Hara, T. Horiguchi, T. Kinoshita, K. Sayama, H. Sugihara, H. Arakawa, *Sol. Energy Mater. Sol. Cells* **2000**, *64*, 115.
[14] Y. W. Zhu, H. Z. Zhang, X. C. Sun, S. Q. Feng, J. Xu, Q. Zhao, B. Xiang, R. M. Wang, D. P. Yu, *Appl. Phys. Lett.* **2003**, *83*, 144.
[15] a) A. M. Morales, C. M. Lieber, *Science* **1998**, *279*, 208; b) Y. Y. Wu, P. D. Yang, *J. Am. Chem. Soc.* **2001**, *123*, 3165; c) J. H. He, J. H. Hsu, C. W. Wang, H. N. Lin, L. J. Chen, Z. L. Wang, *J. Phys. Chem. B* **2006**, *110*, 50.
[16] a) P. M. Gao, Y. Ding, W. J. Mai, W. L. Hughes, C. S. Lao, Z. L. Wang, *Science* **2005**, *309*, 1700; b) H. Y. Peng, N. Wang, X. T. Zhou, Y. F. Zheng, C. S. Lee, S. T. Lee, *Chem. Phys. Lett.* **2002**, *359*, 241; c) X. H. Sun, S. Lam, T. K. Sham, F. Heigl, A. Jürgensen, N. B. Wong, *J. Phys. Chem. B* **2005**, *109*, 3120.
[17] a) Z. W. Pan, Z. R. Dai, Z. L. Wang, *Science* **2001**, *291*, 1947; b) Z. X. Zhang, H. J. Yuan, J. J. Zhou, D. F. Liu, S. D. Luo, Y. M. Miao, Y. Gao, J. X. Wang, L. F. Liu, L. Song, Y. J. Xiang, X. W. Zhao, W. Y. Zhou, S. S. Xie, *J. Phys. Chem. B* **2006**, *110*, 8566.
[18] J. S. Jie, G. Z. Wang, Q. T. Wang, Y. M. Chen, X. H. Han, X. P. Wang, J. G. Hou, *J. Phys. Chem. B* **2004**, *108*, 11976.
[19] a) J. H. Choy, E. S. Jiang, J. H. Won, J. H. Chung, D. J. Jang, Y. W. Kim, *Adv. Mater.* **2003**, *15*, 1911; b) Q. C. Li, V. Kumar, Y. Li, H. T. Zhang, T. J. Marks, R. P. H. Chang, *Chem. Mater.* **2005**, *17*, 1001; c) H. Zhang, D. R. Yang, Y. J. Ji, X. Y. Ma, J. Xu, D. L. Que, *J. Phys. Chem. B* **2004**, *108*, 3955; d) Z. Wang, X. F. Qian, J. Yin, Z. K. Zhu, *Langmuir* **2004**, *20*, 3441.
[20] a) S. Y. Gao, H. J. Zhang, X. M. Wang, R. P. Deng, D. H. Sun, G. L. Zheng, *J. Phys. Chem. B* **2006**, *110*, 15847; b) P. Li, Y. Wei, H. Liu, X. K. Wang, *Chem. Commun.* **2004**, 2856; c) B. Liu, H. C. Zeng, *J. Am. Chem. Soc.* **2004**, *126*, 16744; d) B. Liu, H. C. Zeng, *Langmuir* **2004**, *20*, 4196.
[21] a) B. Liu, H. C. Zeng, *J. Am. Chem. Soc.* **2003**, *125*, 4430; b) X. D. Gao, X. M. Li, W. D. Yu, *J. Phys. Chem. B* **2005**, *109*, 1155; c) M. S. Mo, J. C. Yu, L. Z. Zhang, S.-K. A. Li, A. *Adv. Mater.* **2005**, *17*, 756; d) Y. Sun, G. M. Fuge, N. A. Fox, D. J. Riley, M. N. R. Ashfold, *Adv. Mater.* **2005**, *17*, 2477; e) L. F. Xu, Y. Guo, Q. Liao, J. P. Zhang, D. S. Xu, *J. Phys. Chem. B* **2005**, *109*, 13519.
[22] a) H. D. Yu, Z. P. Zhang, M. Y. Han, X. T. Hao, F. R. Zhu, *J. Am. Chem. Soc.* **2005**, *127*, 2378; b) L. Vayssieres, *Adv. Mater.* **2003**, *15*, 464; c) X. F. Wu, H. Bai, C. Li, G. W. Lu, G. Q. Shi, *Chem. Commun.* **2006**, 1655.
[23] a) Y. P. Fang, Q. Pang, X. G. Wen, J. N. Wang, S. H. Yang, *Small* **2006**, *2*, 612; b) Y. H. Tong, Y. C. Liu, L. Dong, D. X. Zhao, J. Y. Zhang, Y. M. Lu, D. Z. Shen, X. W. Fan, *J. Phys. Chem. B* **2006**, *110*, 20263; c) X. G. Wen, Y. P. Fang, Q. Pang, C. L. Yang, J. N. Wang, W. K. Ge, K. S. Wong, S. H. Yang, *J. Phys. Chem. B* **2005**, *109*, 15303.
[24] a) C. H. Lu, L. M. Qi, J. H. Yang, L. Tang, D. Y. Zhang, J. M. Ma, *Chem. Commun.* **2006**, 3551; b) S. Kar, A. Dev, S. Chaudhuri, *J. Phys. Chem. B* **2006**, *110*, 17848; c) S. Kar, B. N. Pal, S. Chaudhuri, D. Chakravorty, *J. Phys. Chem. B* **2006**, *110*, 4605.
[25] Y. H. Tong, Y. C. Liu, C. L. Shao, Y. X. Liu, C. S. Xu, J. Y. Zhang, Y. M. Lu, D. Z. Shen, X. W. Fan, *J. Phys. Chem. B* **2006**, *110*, 14714.
[26] Y. Liu, Y. Chu, M. Y. Li, L. L. Li, L. H. Dong, *J. Mater. Chem.* **2006**, *16*, 192.
[27] A. Mitra, R. K. Thareja, *J. Appl. Phys.* **2001**, *89*, 2025.
[28] a) D. H. Zhang, Q. P. Wang, Z. Y. Xue, *Appl. Surf. Sci.* **2003**, *207*, 20; b) K. Vanheusden, W. L. Warren, C. H. Seager, D. K. Tallant, J. A. Voigt, B. E. Gnade, *J. Appl. Phys.* **1996**, *79*, 7993.
[29] M. H. Huang, Y. Wu, H. Feick, N. Tran, E. Weber, P. Yang, *Adv. Mater.* **2001**, *13*, 113.

Received: December 18, 2006
Published online: May 30, 2007

